

Identification of Small Molecule Inhibitors Targeting Phosphoserine Phosphatase: A Novel Target for the Development of Antiamoebic Drugs

Poonam Kumari,* Prakhar Agrawal, Preeti Umarao, Vijayan Ramachandran, and Samudrala Gourinath*



Cite This: *ACS Omega* 2024, 9, 27906–27918



Read Online

ACCESS |



Metrics & More

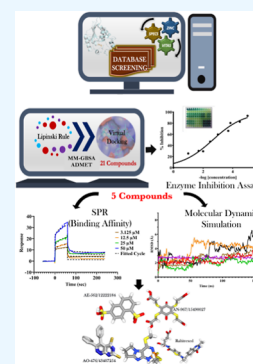


Article Recommendations



Supporting Information

ABSTRACT: Amoebiasis, a widespread disease caused by the protozoan parasite *Entamoeba histolytica*, poses challenges due to the adverse effects of existing antiamoebic drugs and rising drug resistance. Novel targeted drugs are in need of the hour to combat the prevalence of this disease. Given the significance of cysteine for *Entamoeba* survival, the rate-determining step in the serine (the sole substrate of cysteine synthesis) biosynthetic pathway, i.e., the conversion of 3-phosphoserine to L-serine catalyzed by phosphoserine phosphatase (PSP), emerges as a promising drug target. Our previous study unveils the essential role of EhPSP in amoebas' survival, particularly under oxidative stress, by increasing cysteine production. The study also revealed that EhPSP differs significantly from its human counterpart, both structurally and biochemically, highlighting its potential as a viable target for developing new antiamoebic drugs. In the present study, employing *in silico* screening of vast natural and synthetic small chemical compound libraries, we identified 21 potential EhPSP inhibitor molecules. Out of the 21 compounds examined, only five could inhibit the catalytic activity of EhPSP. The inhibition capability of these five compounds was subsequently validated by *in silico* binding free energy calculations, SPR-based real-time binding studies, and molecular simulations to assess the stability of the EhPSP–inhibitor complexes. By identifying the five potential inhibitors that can target cysteine synthesis via EhPSP, our findings establish EhPSP as a drug candidate that can serve as a foundation for antiamoebic drug research.



1. INTRODUCTION

Entamoeba histolytica, a protozoan pathogen, is widespread in countries with inadequate sanitation and hygiene, impacting millions of individuals worldwide.¹ Each year, there are approximately 2.2 million infections, resulting in 55,000 deaths due to amoebiasis.² For several decades, clinicians have relied on metronidazole or its derivative as the primary treatment, often considered the gold standard. However, metronidazole's low efficacy against the latent cyst stage of *E. histolytica* is a matter of concern,^{3,4} necessitating its combination with luminal agents like paromomycin, iodoquinol, or diloxanide.^{5,6} Metronidazole also poses various side effects, such as nausea, vomiting, and neurological symptoms like dizziness, vertigo, and encephalopathy.^{7,8} However, the emergence of metronidazole resistance in recent years has prompted active research into understanding the molecular mechanisms of resistance and identifying new drug targets.^{9–11} Recently, nitazoxanide and aurano-fin have emerged as potential alternative treatments.^{12–14} The challenges posed by resistance, low efficacy, side effects, and adaptation to new drugs like aurano-fin¹³ indicate a need to develop drugs with novel mechanisms of action that target critical pathways in the parasite, which differ significantly from the host.^{4,15–18}

Entamoeba, an extracellular microaerophilic parasite, possesses a robust detoxification system to keep reactive oxygen species (ROS) in check, as high ROS levels are fatal to its existence.^{19,20} A prime example supporting this notion is the

widely used drug metronidazole, which targets the antioxidative machinery of the parasite.²¹ Metronidazole, a prodrug, remains inactive until taken up and reduced. Inside the parasite, its reduction is facilitated by the pyruvate/ferredoxin oxidoreductase system, and the reduced forms, such as the nitroso-free radical and hydroxylamine derivatives,²² are cytotoxic and induce DNA single and double-strand breaks.^{23,24} Activated metronidazole also targets lipids and forms covalent adducts with various cellular proteins, including enzymes responsible for maintaining ROS levels,²⁵ thereby rendering these proteins nonfunctional. Inactivation of such enzymes disrupts cellular ROS homeostasis, causing a surge in free oxygen radicals, ultimately leading to the parasite's death.

Interestingly, metronidazole resistance in *Entamoeba* is associated with a marked increase in the levels of antioxidant enzymes, for example, superoxide dismutase and peroxiredoxin.^{9,26,27} This suggests that ROS detoxification components could be potential targets for developing protein-based therapeutic candidates against *Entamoeba* infections.^{28–30}

Received: November 27, 2023

Revised: January 25, 2024

Accepted: January 31, 2024

Published: June 17, 2024



Additionally, *Entamoeba*'s antioxidant pathways are unique and differ entirely from the host.^{30,31} For example, *Entamoeba* utilizes cysteine as its primary antioxidant rather than glutathione, the principal antioxidant in humans.^{32–34} Furthermore, cysteine also protects the parasite against metronidazole and auranofin, allowing the amoebae to survive at otherwise lethal drug concentrations.³⁸ Cysteine is also known to regulate redox balance in other microaerophilic parasites, i.e., *Giardia lamblia* and *Trichomonas vaginalis*,^{20,35} and for some pathogenic bacteria, including *Staphylococcus aureus*,³⁶ *Mycobacterium tuberculosis*,^{37,38} *Lactobacillus fermentum*,³⁹ and *Bacillus subtilis*.^{40,41} The importance of cysteine's antioxidant role in primitive organisms^{32,42} led to the characterization of its biosynthetic pathway at structural and functional levels. The deep understanding further promoted active research, and various components of this machinery are targeted in pathogens such as *M. tuberculosis*,⁴³ *Salmonella typhimurium*,⁴⁴ *Brucella abortus*,⁴⁵ viruses such as *Haemophilus influenzae*,⁴⁶ parasite protozoan *Leishmania donovani*,^{46,47} and *E. histolytica*.^{18,48–50}

In the *de novo* cysteine biosynthetic pathway of *Entamoeba*, L-serine, the sole substrate, is first synthesized by a set of three enzymes, namely, phosphoglycerate dehydrogenase (PGDH), phosphoserine aminotransferase (PSAT), and phosphoserine phosphate (PSP).⁵¹ The conversion of 3-phosphoserine to serine (final step), mediated by PSP, is an irreversible and rate-limiting step in the serine synthesis pathway and the connecting link between serine and cysteine production. Consequently, targeting this enzyme could effectively control cysteine production in *Entamoeba*, thereby reducing its ability to survive in the human host, particularly under oxidative stress.

Serine biosynthetic pathway has been extensively studied in amoeba, specifically the first two enzymes, PGDH and PSAT,^{52–61} with little emphasis on the third enzyme, i.e., PSP.⁶² Recently, for the first time, our laboratory has identified and characterized PSP from *Entamoeba* (denoted as EhPSP) at biochemical, molecular, structural, and functional levels^{51,63} and has shown its essentiality in the survival and proliferation of amoeba. The work also demonstrated that EhPSP protects the parasite from oxidative stress. Besides, as a druggable target, EhPSP differs markedly from human PSP. First, they belong to distinct superfamilies; EhPSP is a member of the histidine phosphatase superfamily, whereas human PSP belongs to the haloacid dehalogenase-like hydrolase superfamily. Second, they carry out dephosphorylation reactions through distinct mechanisms, each involving different catalytic residues. Lastly, notable structural deviations were observed, and sequence conservation stands at a mere 20%,^{51,63} highlighting the potential of EhPSP as a promising drug target.

In continuation of our previous work, in this report, we conducted a stringent structure-based virtual screening, followed by validation using multiple methods: molecular docking, ΔG of binding free energy calculations, *in vitro* inhibition kinetic assays, real-time binding studies using surface plasmon resonance (SPR), and an assessment of the stability of the EhPSP–inhibitor complex employing molecular simulations. By combining computational tools and *in vitro* assays, this study identifies five lead molecules targeting EhPSP and provides enough pieces of evidence that EhPSP can be taken as a drug target for future anti-amoebic drug discovery.

2. MATERIALS AND METHODS

2.1. Protein and Ligand Formulation for Docking.

Virtual screening was conducted using the Vitas-M, Specs, and

Zinc databases containing small molecules and natural compounds. The small molecule libraries were obtained as a 2D-structure data file (SDF). The LigPrep module of Schrödinger software was employed to prepare the libraries for docking. This module utilized the OPLS 2005 force field and the Epik ionizer at a standard pH of 7.4, ensuring the conversion of compounds into low-energy 3D structures with correct chirality.⁶⁴ The maximum number of conformers per structure was 32, with a root-mean-square deviation (RMSD) of 1.0.

The EhPSP structure (PDB ID: SZKK) was imported from the Protein Data Bank (PDB) into the maestro workflow. The Protein Preparation Tool of Schrödinger software was used to prepare the protein. This involved filling in missing side chains through homology modeling (Prime module), removing water located more than 3 Å from protein residues, optimizing hydrogen bonds, and assigning charges to atoms using the OPLS3 force field. The minimization process was terminated when the maximum RMSD for atom displacement reached 0.30 Å.

2.2. Grid Generation. The SiteMap module was utilized to identify potential binding sites for compounds. Among the identified sites, the substrate binding site, which was determined based on the complex crystal structures of EhPSP-O-phospho-L-serine (OPLS) and EhPSP-3-phosphoglyceric acid (3PG) substrate, was ranked the highest for ligand binding studies. The ranking was determined by evaluating the SiteScore and Dscore, and the substrate binding site exhibited a SiteScore value of 0.973 and a Dscore value of 0.853, with a volume of 226.72 Å. On the other hand, the remaining identified sites had volumes smaller than 100 Å and SiteScore and Dscore values below 0.7. Consequently, the substrate binding site was selected as the docking site for the compounds. In the energy-minimized EhPSP structure, a receptor grid was created to cover all of the residues within the active site of EhPSP.

2.3. In Silico Screening of Potential Inhibitors against EhPSP. The docking studies were conducted using the Glide module of Schrödinger software, following the approach described in Friesner et al. (2006).⁶⁵ The high-throughput virtual screening (HTVS) precision mode was initially employed to dock the compound library. This mode operated at a faster rate of 2 s per compound, prioritizing speed over accuracy. Subsequently, the top 10% of the compounds from the HTVS output was further analyzed using the extra precision (XP) mode, which performs exhaustive sampling, leading to higher accuracy in the docking results. Additionally, the XP mode considers positive and negative interactions by rewarding and penalizing them, which is reflected in the docking output file.

2.4. Calculation of the Binding Energy Via Prime MM-GBSA. The XP docking poses were utilized for calculating ligand binding free energies, and the calculations were performed by using the prime MM-GBSA approach. MM-GBSA, which stands for molecular mechanics-generalized Born model and solvent accessibility, is employed to investigate the energetics of biomolecular systems.⁶⁶ MM-GBSA calculates the relative free energy of the protein, ligand, and protein–ligand complex according to the equation given below

$$\text{binding free energy } (\Delta G_{\text{bind}}) = \Delta G_{\text{solv}}, \Delta E_{\text{MM}}, \text{ and } \Delta G_{\text{SA}}$$

$$1. \Delta G_{\text{bind}} (\text{MM-GBSA } \Delta G_{\text{bind}}) = \text{energy of complex} - (\text{receptor energy} + \text{ligand energy})$$

2. ΔG_{solv} represents the difference in GBSA solvation energy between the protein–ligand complex and the sum of the apoprotein and ligand solvation energies.
3. ΔE_{MM} indicates the difference in minimized energies between the protein–ligand complex and the sum of the energies of the apoprotein and ligand.
4. ΔG_{SA} represents the difference in surface area energies between the complex and the sum of the surface area energies of the apoprotein and ligand.

The ΔG_{solv} , ΔE_{MM} , and ΔG_{SA} terms contribute to the overall binding free energy determination using the MM-GBSA method.

2.5. Overexpression and Purification of EhPSP.

Expression and purification of the recombinant EhPSP protein was conducted following the procedures described in our previous paper.⁵¹ Briefly, the EhPSP gene was cloned into the pET-28(b) vector with a 6X-His tag at the C-terminus of the protein. The resulting recombinant pET-28(b)-EhPSP plasmid was transformed into *Escherichia coli* BL21 (DE3) cells for overexpression and subsequently purified using a two-step method. The first step involved Ni-NTA affinity chromatography, followed by size exclusion chromatography (SEC). The purified protein was further utilized for the inhibition assays.

2.6. In Vitro Enzyme Inhibition Assay. Based on the availability, shortlisted potential compounds were purchased (details are provided in Table S1) and were evaluated for their effect on the phosphatase activity of EhPSP using OPLS as the substrate by the Baykov malachite green method.⁶⁷ A standard reaction mixture of 100 μL was prepared for the inhibition assay consisting of 50 mM HEPES-NaOH buffer (pH 8.0), 1 mM DTT, 1 mM EDTA, and 25 μg of purified EhPSP protein. Varying concentrations of drug-like compounds were added to the reaction mixture, followed by incubation at room temperature (RT) for 10 min. Post-incubation, OPLS was added at a final concentration of 2.0 mM to initiate the reaction and was further incubated at RT for an additional 2–5 min, following the same conditions as the native phosphatase assay for EhPSP.⁵¹

Furthermore, a volume equal to one part (i.e., 25 μL) of malachite green dye solution was added to the reaction mixture to halt the reaction. As a result, a blue phosphomolybdate complex was formed, and the concentration of the released inorganic phosphate was determined by measuring the absorbance of the reaction mixture at 630 nm using a microplate reader (Thermo Scientific Varioskan Flash). The absorbance, directly proportional to the amount of inorganic phosphate formed, was an indicator of the activity level.

The absorbance of the standard reaction (i.e., reaction with enzyme and substrate only) was compared with the ones with the compound, and the percentage of inhibition was calculated as a percentage decrease in activity using the following equation

$$\% \text{inhibition} = 100 - \frac{A_{630} \text{ in presence of compounds}}{A_{630} \text{ in absence of compounds}} \times 100$$

A concentration-dependent inhibition curve was generated to determine the half-maximum inhibitory concentration (IC₅₀) value. The compound concentrations were varied from 20 nM to 500 μM while maintaining a constant OPLS concentration of 2.0 mM. The data was analyzed and plotted using GraphPad Prism 5.0.⁶⁸

2.7. Binding Studies Using Surface Plasmon Resonance. SPR-based interaction analysis was conducted by using a

Biacore T200 instrument from GE Healthcare. To immobilize EhPSP, a concentration of 50 $\mu\text{g}/\text{mL}$ was utilized, and the amine coupling method was employed on a CMS chip. The binding of the potential compounds with EhPSP was evaluated using a multicycle kinetic procedure in a solution of 1 \times PBS supplemented with 5% DMSO and 0.05% Tween-20. To account for solvent effects, a standard curve of DMSO was included for solvent correction. The changes in resonance units (RUs) over time were used to report biomolecular binding events. The binding affinity was determined by using the Biacore T200 evaluation software, employing a 1:1 binding model.

2.8. Molecular Dynamic Simulations. To evaluate the stability of the protein–inhibitor complexes, molecular dynamics (MD) simulations were conducted using the Desmond module of Schrödinger software.⁶⁹ The process involved solvating the complexes using the TIP4PEW solvation model while maintaining a NaCl concentration of 0.15 M to ensure a physiological ionic strength. After solvation, the complexes were subjected to energy minimization, and the simulation was performed for 150 ns. The final frame of the simulation was saved in a PDB file format. To analyze the intermolecular interactions between the protein and the inhibitor atoms, the complexes were loaded into the LigPrep workspace of Schrödinger (version 2021-3), and LigPlot^{70,71} was used to generate the schematic representations of these interactions.

2.9. Theoretical Prediction of the ADMET Parameters of the Compounds. Drug likeness represents a delicate equilibrium of diverse molecular properties and structural characteristics. Consequently, the compounds that showed enzyme inhibition were subjected to the theoretical prediction of their pharmacokinetic properties based on their molecular structure using the QikProp and Swiss absorption, distribution, metabolism, excretion, and toxicity (ADMET) online server (<http://www.swissadme.ch/>).⁷² To perform the analysis, the server required the SMILES representation of each compound and predicted various ADMET parameters referred to as absorption, distribution, metabolism, and excretion/elimination. Additionally, it evaluated the drug-like nature of the compounds and their medicinal chemistry based on Lipinski's rule of five.

3. RESULTS

3.1. Molecular Docking Studies. To identify potential inhibitor molecules, we employed crystallographic structures obtained from the EhPSP protein complexed with OPLS [PDB ID:5ZR2] and 3PG [PDB ID: 6M1X]^{51,63} substrates. Docking was performed at the substrate binding site with three libraries containing small molecules and natural compounds: Vitas-M, Specs, and Zinc database. The rigid docking of compounds on the active site of EhPSP led to the identification of molecules with docking scores < -0.098 and binding affinities < -15.06. However, based on the commercial availability of the compounds, the top 21 molecules were selected for further study. Table S1 (Database ID, IUPAC nomenclature, and molecular weight) and Table S2 (Docking and MM-GBSA score) contain detailed information about the tested compounds.

3.2. Enzyme Inhibition Assay Identifies Five Molecules as Potential Inhibitors. The 21 molecules selected from the docking study were tested for their inhibitory effects on EhPSP *in vitro*. Inhibition studies were performed to measure the decrease in the enzymatic activity by observing the rate of

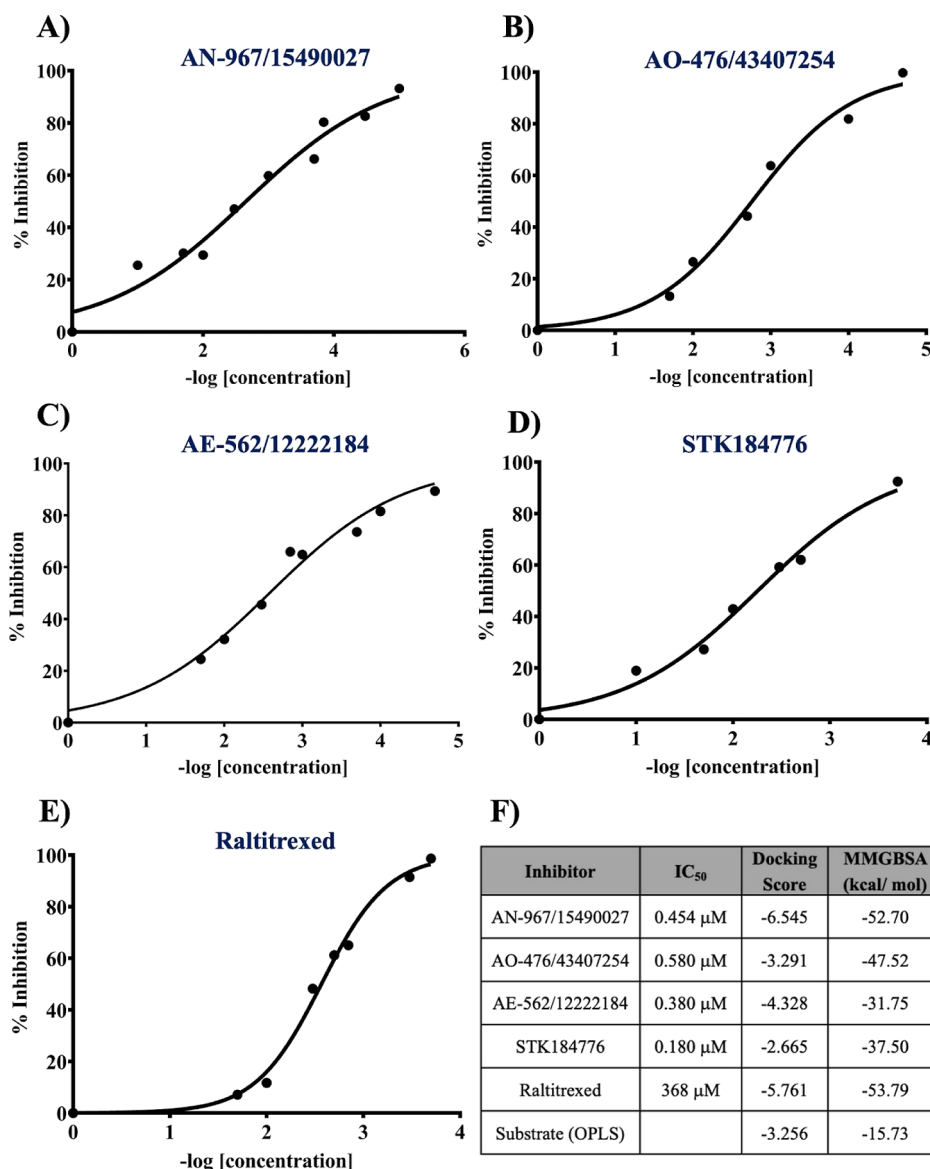


Figure 1. Enzyme inhibition activity with different compounds. Plot for % inhibition versus the log of inhibitor concentrations for EhPSP. Inhibition curves for (A) AN-967/15490027, (B) AO-476/43407254, (C) AE-562/12222184, (D) STK184776, and (E) raltitrexed at various concentrations. (F) Tabulated IC₅₀ values, docking scores, and MM-GBSA values (ΔG of binding).

conversion of phosphoserine to serine. IC₅₀ values for each compound were calculated by measuring the normalized inhibition with increasing log inhibitor concentrations. Out of the 21 compounds tested, five of them (AN-967/15490027, AO-476/43407254, AE-562/12222184, STK184776, and raltitrexed) displayed the inhibition of enzymatic activity. The hydrolysis rate of the substrate was significantly reduced in a dose-dependent manner in the presence of these compounds (Figure 1). The IC₅₀ values for these compounds were found to be 180 to 580 nM (Figure 1F), except for raltitrexed, which exhibited an IC₅₀ value of approximately 368 μM.

The maximum inhibition observed for all of these compounds was 80–90% of EhPSP enzymatic activity. This indicates that the *in vitro* inhibition assay results are consistent with the theoretical observations obtained through molecular docking. Figure 2 provides the chemical structures of all five potential compounds.

3.3. Mapping the Interactions of Potential Inhibitors with EhPSP's Active Site. Furthermore, the interactions

between five potential inhibitors and the active site of EhPSP were analyzed. The conformations with the lowest docking score were chosen, and the interactions were plotted by using Lig-Plot. A superimposed view of the binding poses of potential inhibitors in the active site of EhPSP is represented in Figure 3, whereas Figure S1 demonstrates the individual binding of all compounds.

A comparative analysis was performed between the interactions observed for these compounds and those present in the crystal structure of the EhPSP-OPLS complex. OPLS interacts with EhPSP largely by hydrogen bonding involving the following residues: Arg8, His9, Gln21, Gly22, Arg57, and Gly147, as well as hydrophobic interactions (Ile20, Glu79, Phe82, and His146) as shown in Figure 4A. Interestingly, compounds AN-967/15490027, AE-562/12222184, and raltitrexed exhibited nearly similar interactions with the binding pocket residues (Figure 4). For example, AE-562/12222184 formed hydrogen bonds with Arg8, Asn15, Gln21, Arg57, His146, and Gly147, along with hydrophobic interactions involving Gly22, Glu79, and Phe82.

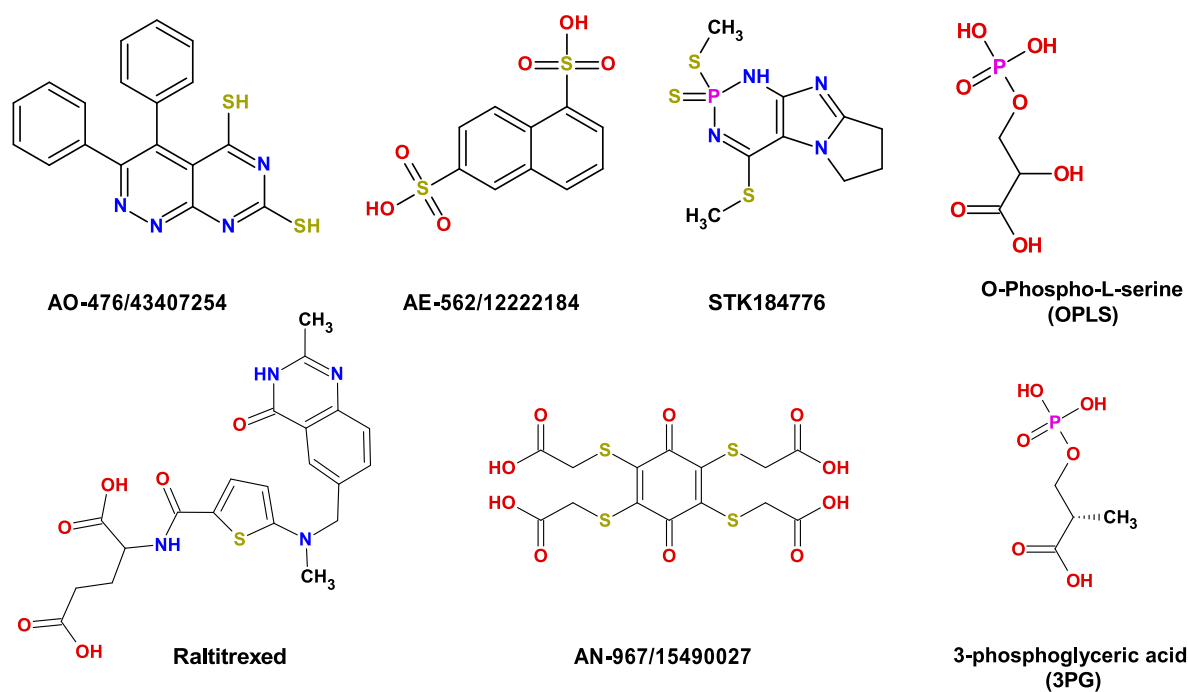


Figure 2. 2D configuration of the lead molecules and substrate of EhPSP. The identified potential molecules belonged to diverse classes, such as AO-476/43407254, a phenylpyridazine; AE-562/12222184, a naphthalenesulfonate; STK184776, an azole; raltitrexed, a quinoline folate analogue; and AN-967/15490027, an alkaloid.

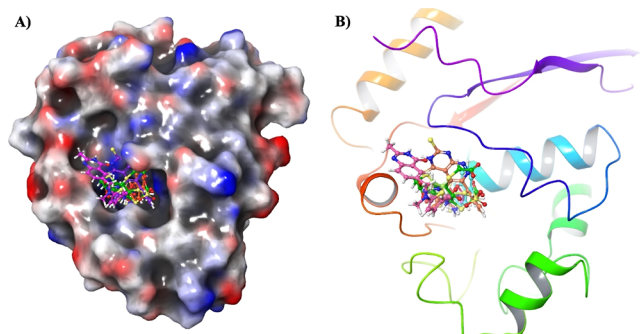


Figure 3. 3D representation displaying the binding poses of the potential inhibitors within the active site of EhPSP. EhPSP complexed with OPLS (substrate) and inhibitors AE-562/12222184, AN-967/15490027, raltitrexed, AO-476/43407254, and STK184776. The compounds are displayed as balls and sticks, while the protein is represented in the surface view (A) and cartoon representation (B), with inhibitor molecules in the active site. The figure was generated using Maestro (version 2019-1).

In addition to these interactions, compound AN-967/15490027 engages in hydrogen bonding with Lys151 and Leu170, while raltitrexed forms with Asn172, accompanied by a range of hydrophobic interactions involving residues such as His9, Gly18, Ile20, Phe90, Glu79, Tyr165, etc. Compound STK184776 displayed a comparatively lower number of interactions with the active site, primarily establishing hydrogen bonds with Asn15 and Gln21. On the contrary, AO-476/43407254 exhibited interactions that differ from those observed with the substrate, forming hydrogen bonds with Tyr165, Lys151, and Gln169 and multiple hydrophobic interactions (Ile20, Trp85, Tyr99, Phe102, and Ala148) (Figure 4). Overall, these results demonstrate that all the compounds form a significant number of interactions, implying their potential to compete with the substrate for the active site residue of EhPSP.

Furthermore, to evaluate the specificity of these five potential inhibitors, we carried out molecular docking into the active site of HPSP (PDB ID: 1L8O). The results revealed that none of these compounds exhibited noteworthy interactions with the human counterpart, compared to their interactions with EhPSP (Figure S2), further displaying their specificity toward EhPSP.

3.4. Binding Studies Showed that the Compounds Exhibited Stronger Binding than the Substrate. Developing new molecules requires a meticulous evaluation of their binding affinity with the protein target under consideration. A more negative binding affinity indicates stronger binding of a molecule with its target protein. The ΔG of binding was calculated using the Prime MM-GBSA module, revealing that all the lead inhibitors had lower ΔG values compared to the substrate (Figure 1F), highlighting that the inhibitor has a stronger binding with the active site.

SPR allows real-time measurement of the binding affinity between a ligand and a protein. Therefore, *in silico* binding of potential inhibitors with EhPSP was further confirmed with SPR. To measure the binding affinity, EhPSP was immobilized, and the compounds were passed over it. Buffer blanks were injected between cycles for baseline referencing, and the binding sites were regenerated using 10 mM glycine pH 3.0.

The sensorgram analysis shows that AO-476/43407254 and AN-967/15490027 exhibit strong binding to EhPSP, with K_D values of 1.28 and 27.5 μM , respectively, as determined by the 1:1 Langmuir fitting (Figure 5), whereas the substrate OPLS showed weak binding with a K_D value of 20 mM. On the other hand, the remaining three inhibitors, namely, STK184776, AE-562/12222184, and raltitrexed, were found to be interacting with the chip; therefore, their binding affinity could not be determined.

3.5. MD Simulation Studies of the EhPSP–Inhibitor Complexes. A MD simulation was carried out to understand the lead inhibitors' stability in the protein's catalytic site. MD

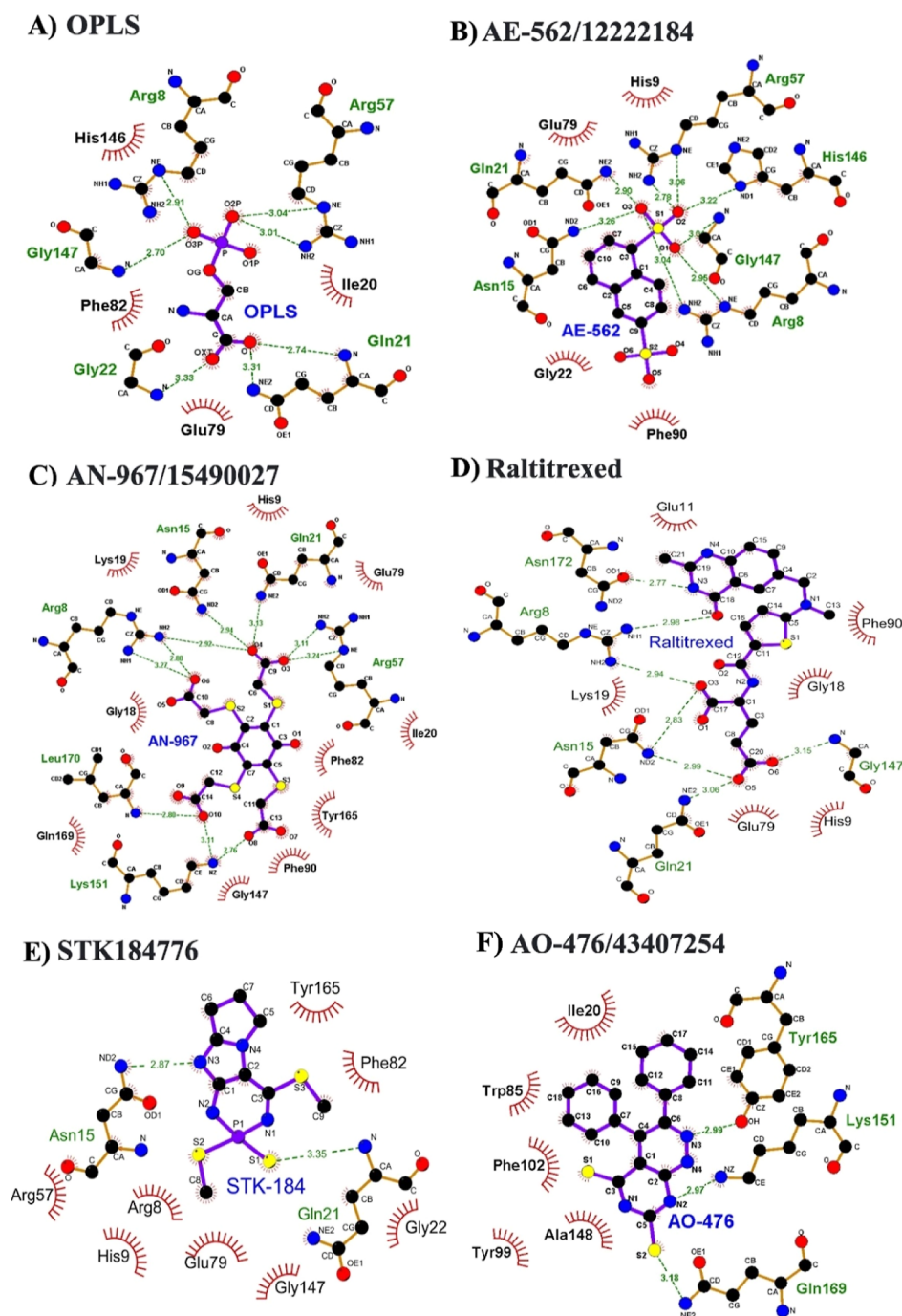


Figure 4. Illustration of the interactions between potential inhibitors and the active site residues of EhPSP. Interactions are plotted for substrate (A) OPLS and compounds (B) AE-562/12222184, (C) AN-967/15490027, (D) raltitrexed, (E) STK184776, and (F) AO-476/43407254. The figure was generated by using LigPlot. Hydrogen bonds are represented by dashed lines between the atoms involved, while hydrophobic contacts are depicted as an arc with spokes radiating toward the ligand atoms they interact.

simulations were performed for EhPSP-OPLS and all five EhPSP–inhibitor complexes for 150 ns. The stability of each residue in the protein–ligand complexes was assessed by calculating the protein backbone’s root-mean-square fluctuations (RMSFs). The RMSF plots illustrate that the protein residues exhibited minimal fluctuations (~ 1 Å) in different complexes (Figure 6A), particularly for a few residues, like Leu17, Gly18, Asp68, Glu91, Asp96, Thr114, and Gly115.

Among all of the protein–ligand complexes, the EhPSP-AO-476/43407254 and EhPSP-STK184776 complexes exhibited slightly higher fluctuations in certain other residues as well, such

as Ile74, Glu75, Gly76, Glu79, Ser104, and Thr114. On the other hand, the AE-562/12222184 in complex with EhPSP displayed the highest stability with the lowest fluctuations throughout the simulation. However, during the 150 ns simulation, all complexes maintained structural stability around the ligand binding residues, including Arg8, His9, Asn15, Phe82, and Phe90 (Figure 6A).

To assess the overall stability of the complexes, the RMSD of the protein backbone was calculated by considering the initial backbone coordinates of the protein–ligand complexes as the reference. The RMSD plot indicated a standard deviation of less

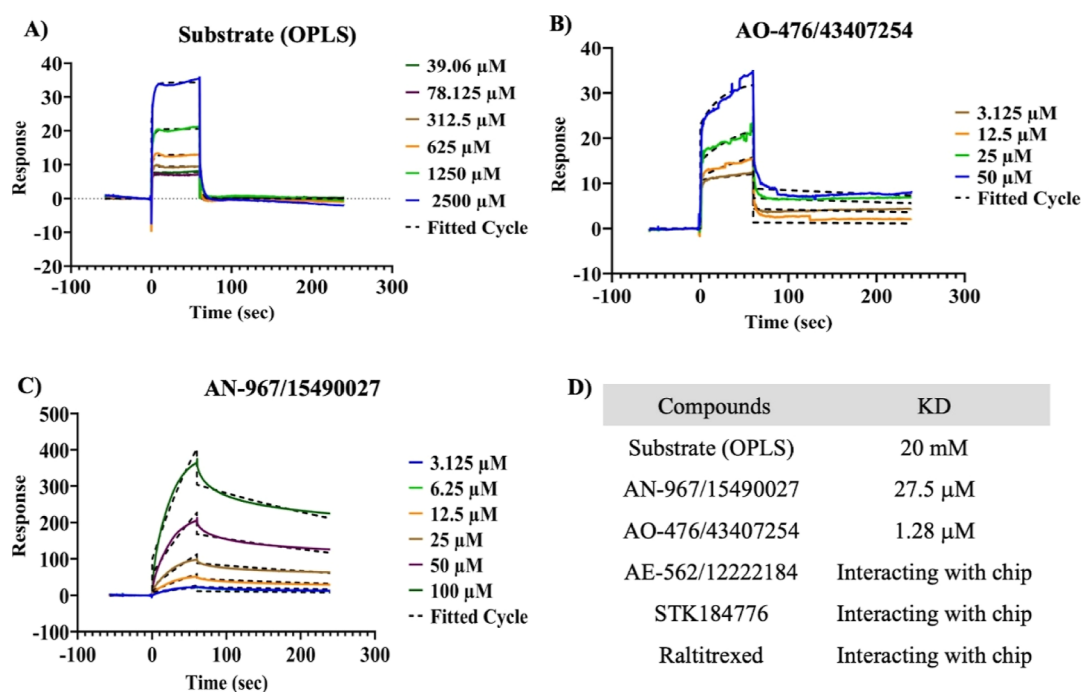


Figure 5. Binding studies of EhPSP with the substrate OPLS and inhibitors using SPR. The sensorgram depicting binding responses for the (A) substrate OPLS and small molecules (B) AO-476/43407254 and (C) AN-967/15490027 at different concentrations. (D) Tabular representation of the dissociation constant (K_D) values of the substrate and two inhibitors.

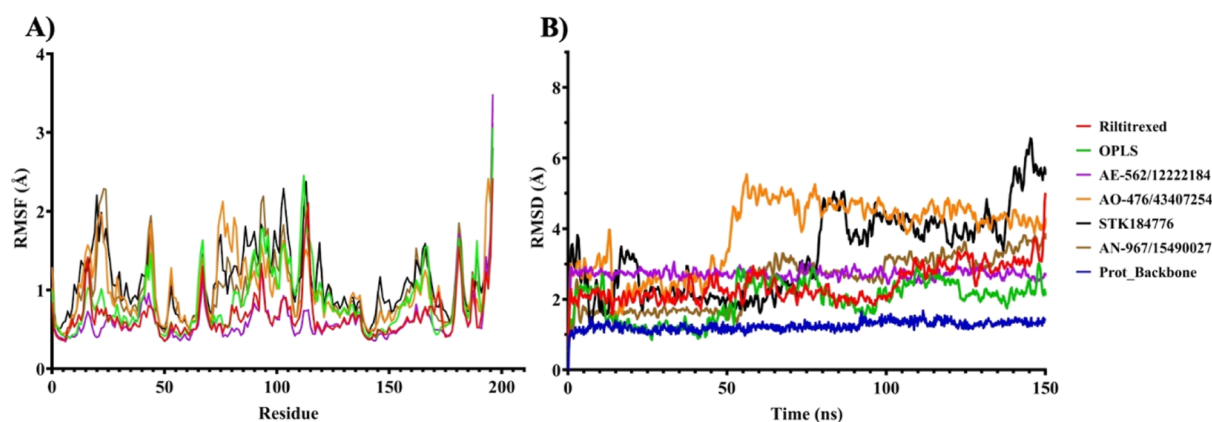


Figure 6. MD simulations of EhPSP–potential inhibitor complexes. Panel (A) illustrates the RMSF trajectory analysis of the backbone atom within the EhPSP–inhibitor complexes, while panel (B) presents the RMSD plotted against time for the EhPSP–inhibitor complexes. RMSD and RMSF were computed based on the initial and final conformation differences. The graphs encompass various runs, with the unbound EhPSP shown in blue, OPLS in green, AO-476/43407254 in a distinctive yellow shade, STK184776 in black, raltitrexed in red, AE-562/12222184 in purple, and AN-967/15490027 in algal green blue.

than 2 Å, indicating relatively stable interactions throughout the simulation (Figure 6B). However, the EhPSP-AO-476/43407254 complex exhibited a slightly higher deviation than the others. The association of EhPSP with the STK184776 compound remained stable for the initial 80 ns but experienced a relatively higher RMSD thereafter, suggesting a potential diffusion of STK184776 away from the binding site. In contrast, the EhPSP-AE-562/12222184 complex displayed the least deviation among all of the complexes throughout the simulation (Figure 6B).

Furthermore, various interactions between ligand and active site residues, including water bridges, pi–pi, and ionic interactions, were mapped for all of the complexes throughout the simulation, and the resulting histograms illustrated the variations in the RMSD values. It was observed that OPLS, AE-

562/12222184, and AN-967/15490027 maintained hydrogen bond and water bridge interactions for nearly 100% of the simulation time, leading to low and stable RMSD values (Figure 7A–C). Raltitrexed also primarily established hydrogen bonds and water bridges with EhPSP, along with hydrophobic interactions, although these interactions were relatively sustained for shorter intervals (Figure 7E).

Compared to the aforementioned complexes, AO-476/43407254 and STK184776 exhibit similar modes of interactions and display a reduction in water bridge interactions while majorly forming stronger bonds, such as ionic, pi–pi, and hydrophobic interactions. The strength and duration of the interactions are comparatively lower (Figure 7D,F). Nevertheless, the number and strength of these interactions were

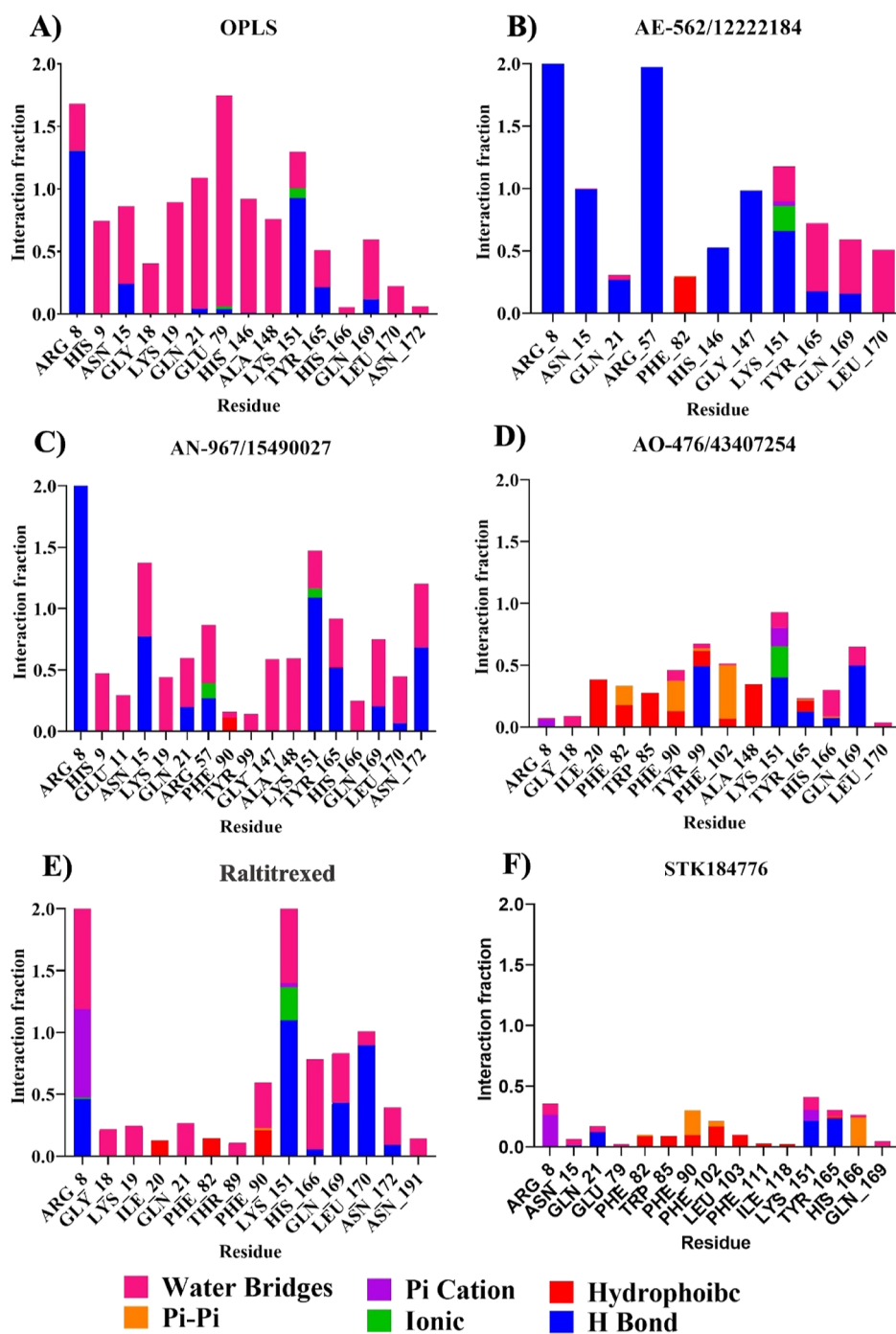


Figure 7. Histogram depicting various interactions and their respective levels between the potential inhibitors and the binding pocket of EhPSP, as monitored throughout the simulations. The panel represents the interactions of the binding pocket of EhPSP with the compounds: (A) OPLS, (B) AE-562/12222184, (C) AN-967/15490027, (D) AO-476/43407254, (E) raltitrexed, and (F) STK184776.

Table 1. ADMET Parameter Values for Lead Molecules Calculated Using QikProp

compound name	MW	donor HB	acceptor HB	QPlogPo/w	QPCCaco	QPlogBB	QPMDCK	% human oral absorption	rule of five
AE562/12222184	288.29	2	8	0.316	2.203	-1.912	1.127	34.935	0
AN967/15490027	468.483	4	14	-0.175	0.002	-5.313	0.001	0	0
AO-476/43407254	228.345	2	4	2.025	2618.281	0.515	10 000	100	0
raltitrexed	458.488	3.25	10.25	2.275	0.46	-3.577	0.279	34.235	0
STK184776	304.382	1	4.5	3.121	3754.542	0.4	10 000	100	0

adequate to retain the compounds within the active site of the EhPSP.

3.6. All Potential Inhibitors were Observed to Comply with the ADMET Parameters and Lipinski's Rule. The investigation of ADMET qualities is critical in drug develop-

ment, which aids in predicting the efficacy, safety, and potential adverse effects of the compound. Therefore, all the compounds exhibiting inhibitory activity were subjected to the theoretical prediction of ADMET parameters using Swiss-ADMET (Table S3) and Qikprop (module of the Schrödinger software) (Table 1). These predictions are based on the quantitative structure–activity relationship models, which employ mathematical models to correlate known compound structures with the ADMET properties. It quantifies relationships between structural features and biological activities, assisting in the prediction of the ADMET parameters.

Swiss-ADMET and QikProp indicated that compounds have permissible values for molecular weight (≤ 500 Da), number of hydrogen bond donors (≤ 5), and acceptors (≤ 15). The solubility parameter for potential inhibitors, denoted by QPlogPo/w, was found to be less than 4. Ideally, QPlogPo/w should fall between 5 and 45, indicating its low solubility in water and high solubility in lipophilic solvents. Two independent models, QPPCaco and QPPMDCK (model for gut–blood barrier), were utilized to predict the cellular permeability of compounds measured in nanometers per second with values greater than 500, indicating high permeability. Notably, AO-476/43407254 and STK184776 showed values surpassing 1000.

Furthermore, QPlogBB was employed to predict the transfer of compounds across the blood–brain barrier, where negative values indicate a low transfer rate without active transport. The results showed that except for AO-476/43407254 and STK184776, all other compounds exhibited QPlogBB values less than -1.912 . While AO-476/43407254 and STK184776 had values of approximately 0.5 and 0.4, respectively, suggesting their ability to cross the blood–brain barrier readily, both compounds were found to have 100% human oral absorption values.

Notably, all the potential inhibitors adhered to Lipinski's rule of five and exhibited predicted pharmacokinetic parameters with drug-like characteristics. In conclusion, these results suggest that the *in vitro* potential of these compounds makes them promising candidates for further drug development.

4. DISCUSSION

Amoebiasis poses a significant health concern in developing countries. Considering the growing resistance to current drug treatments, there is a pressing need to explore new targets for effective treatment. The pathogen relies on cysteine for various processes that are crucial for its survival within the human host, including attaching to host epithelial cells, facilitating motility during phagocytosis and pinocytosis, promoting proliferation, gene regulation, and most primarily, defending against oxidative stress.^{34,73–77} Furthermore, the unique cysteine biosynthetic machinery provides a hopeful prospect for discovering potential drug candidates without detrimental effects on the host system;^{18,78,79} therefore, this machinery has been exploited extensively for drug development. However, the enzymes of the serine (exclusive substrate for cysteine synthesis) biosynthesis pathway in *Entamoeba* remain primarily unexplored as potential drug targets. Previously, we demonstrated the significance of EhPSP in parasite growth and in combating oxidative stress. Besides, EhPSP exhibits notable disparities compared to its host counterpart. Similarly, reports on other pathogens, such as *M. tuberculosis* (*Mtb*), show that inhibitors targeting MtbPSP displayed a specific ability to eradicate intracellular *Mycobacte-*

rium efficiently.⁸⁰ Therefore, based on these observations, in the present study, we examined EhPSP as a potential drug target.

In the pursuit, we employed multiple *in silico* and *in vitro* approaches to identify novel small molecules that could serve as a starting point for antiamebic drug discovery. To achieve this, we initially performed an *in silico* screening that allows for rapid screening of an extensive compound library in a short time. The docking studies effectively identify the potential binders within the protein's active site as having higher *in silico* binding affinity than the substrate. Since compound docking involves scoring functions and algorithms that penalize and reward interactions, the results may contain false positives. Besides, the *in silico* binding affinity does not account for solvent or ligand/protein flexibility; thus, the predicted binding affinity may not translate well in biological activity assays. Therefore, the top hits were tested in an enzyme inhibition assay to evaluate their potential as inhibitors of EhPSP's phosphatase activity. Notably, among the 21 compounds tested, only five showed inhibitions of enzymatic activity, and the IC₅₀ values for these inhibitors were measured in the nM range. The result of the enzyme inhibition assay corroborated the analysis from *in silico* docking studies.

Since these five molecules (AE-562/12222184, AN-967/15490027, raltitrexed, STK184776, and AO-476/43407254) were able to displace the substrate from the active site, preventing its conversion to product, their mechanism of inhibition of EhPSP's phosphatase activity was further studied using various computational and *in vitro* tools. Though these methods are used for predicting binding affinity and protein–ligand complex stability or for identifying interacting residues, they may not provide information as precise as the gold standard methods such as NMR or X-ray crystallography. However, computational methods, such as MD simulation, offer valuable insights that reveal key interactions and predict the behavior of protein–ligand complexes under physiological conditions, including information on stability, flexibility, and conformational changes that occur over time.

To understand their competitive inhibition properties, a detailed analysis was performed on the interactions between the five lead compounds and the substrate with the active site residues, which revealed that the lead compounds established similar interactions with the active site residues, as observed in the case of the substrate. However, the compounds exhibited a higher proportion of stronger interactions like the pi–pi interaction and hydrophobic bonds compared to those observed with the substrate, which convincingly elucidates the competition observed in the enzyme inhibition assay.

To further evaluate the strength of interactions, both *in silico* and real-time binding affinity analysis was performed, demonstrating that the inhibitors' binding affinity was significantly lower than that of the substrate. For instance, the substrate (OPLS) exhibited a binding affinity of around -15 kcal/mol, while the compound binding scores measured less than -30 kcal/mol, indicating substantially stronger interactions. A similar pattern was observed in the SPR-based real-time binding affinity determination, corroborating the *in silico* analysis.

Furthermore, MD simulations aided us in better understanding the dynamics of the interactions with the active site residues that evolved over time. It also extended our insights into how ligand binding affected the flexibility of the protein backbone and the overall stability of the protein–ligand complexes. The MD simulation results showed that binding of raltitrexed and AE-562/12222184 led to a reduction in protein

RMSF, whereas STK184776 and AO-476/43407254 binding resulted in relatively higher RMSF, particularly for a few residues in comparison to the substrate (OPLS). Furthermore, the results from the RMSD plots corroborate these observations. Among the five inhibitor–protein complexes, three complexes, notably EhPSP–raltitrexed, EhPSP–AE-562/12222184, and EhPSP–AN-967/15490027, emerged as the most stable complexes, exhibiting minimal fluctuations in terms of RMSD. The binding of STK184776 and AO-476/43407254 demonstrated slightly higher levels of RMSD in comparison with those of other compounds and substrate. The increased fluctuation in protein–ligand complexes for these compounds may be due to the high mobility of ligands in the active site as these compounds also formed a smaller number of hydrogen bonds and water bridges with the active site residues. This was further proved when the real-time interaction with the active site through a course of 150 ns simulations was plotted as stacked bar charts. The comparative analysis revealed that STK184776 and AO-476/43407254 had lower interaction fractions with the active site residues compared with raltitrexed, AE-562/12222184, and AN-967/15490027.

An essential aspect of small molecule identification involves evaluating their potential toxicity parameters, and the selected molecules for *in vitro* toxicity and efficacy studies should have acceptable values for various ADMET parameters. The results of QikProp and Swiss ADMET analyses revealed that all of the molecules met the criteria for an acceptable number of hydrogen bond donors/acceptors. Additionally, none of the molecules violated the Lipinski's rule of five and also demonstrated acceptable pharmacokinetic properties, indicating their potential as lead candidates for future drug development. Moreover, we evaluated the effects of all five potential inhibitors on the growth of the amoebic trophozoites. However, we did not observe any notable inhibitory effect, which could be attributed to a solubility barrier. The compounds were found to precipitate at lower concentrations of DMSO, also supported by the QPlogPo/w values that indicated their low solubility in water and high solubility in lipophilic solvents; this limits our ability to investigate the inhibitory potential on amoebic growth further.

In a broader context, it is worth noting that the results from docking studies, binding affinities, and simulation stability assessments align closely with the outcomes of *in vitro* inhibition assays, further validating the accuracy of the screening protocol utilized. Our systematic approach led to the successful identification of promising seed molecules, thereby laying the foundation for a novel class of anti-amoebic agents targeting the cysteine biosynthetic pathway through EhPSP, a critical aspect of amoebic antioxidant machinery.

In summary, this work tries to identify potential molecules that can target EhPSP and thus serine production, thereby creating a cysteine deficiency that will lead to disruption of oxidative stress management in amoebae. The molecules identified can be further chemically modified to enhance their solubility and efficacy, which may lead to the development of new inhibitors against amoebiasis. Nonetheless, it is critical to emphasize that these predicted binding orientations and interactions should be validated using crystallographic studies and cell-based assays to determine the efficacy of these inhibitors against the novel phosphatase enzyme. Furthermore, integration of our results with experimentally validated data can help in compound selection, optimization, and the development of safer and more efficacious drugs against amoebiasis.

■ ASSOCIATED CONTENT

■ Supporting Information

The Supporting Information is available free of charge at <https://pubs.acs.org/doi/10.1021/acsomega.3c09439>.

Details of the molecules tested for EhPSP inhibition with the potential compound highlighted in light orange color; docking parameters for the molecules tested for EhPSP inhibition with the potential compound highlighted in light orange color; theoretical prediction of ADMET parameters for all the potential compounds; cartoon representation of the binding poses for all the potential compounds within the active site of EhPSP; and molecular docking of the potential compounds in the active site of the HSPS protein (PDF)

■ AUTHOR INFORMATION

Corresponding Authors

Poonam Kumari – International Centre for Genetic Engineering and Biotechnology, New Delhi 110067, India; Structural Biology Lab, School of Life Sciences, Jawaharlal Nehru University, New Delhi 110067, India; orcid.org/0000-0001-9590-929X; Email: sgourinath@mail.jnu.ac.in

Samudrala Gourinath – Structural Biology Lab, School of Life Sciences, Jawaharlal Nehru University, New Delhi 110067, India; orcid.org/0000-0003-4090-3063; Email: poonam.bio12@yahoo.co.in

Authors

Prakhar Agrawal – International Centre for Genetic Engineering and Biotechnology, New Delhi 110067, India; orcid.org/0000-0003-3641-4814

Preeti Umarao – Structural Biology Lab, School of Life Sciences, Jawaharlal Nehru University, New Delhi 110067, India

Vijayan Ramachandran – The Centre for Innovation in Brain Sciences, University of Arizona, Tucson 85721 Arizona, United States

Complete contact information is available at: <https://pubs.acs.org/10.1021/acsomega.3c09439>

Author Contributions

P.K. and S.G. contributed to the conception and design of the study. V.R. conducted the database screening and analysis for the inhibitor molecules, while P.K. and P.A. further did the computational aspects of the research. P.K. and P.U. conducted the wet lab experiments and analyzed the data. P.A. performed the SPR-based experiments. P.K. drafted the first draft of the manuscript. P.U. and P.A. contributed to editing the manuscript subsequently. All authors participated in revising the manuscript, reading, and approving the final submitted version.

Notes

The authors declare no competing financial interest.

■ ACKNOWLEDGMENTS

S.G. is thankful for the SERB-STAR grant. P.K. and P.U. thank the DBT-MK BHAN Postdoctoral Fellowship and ICMR-SRF, India, respectively, for providing them with their fellowships.

■ REFERENCES

- (1) Debnath, A.; Rodriguez, M. A.; Anki, S. Editorial: Recent Progresses in Amebiasis. *Front. Cell Infect. Microbiol.* **2019**, *9*, 247.

- (2) Turkeltaub, J. A., 3rd; McCarty, T. R.; Hotez, P. J.; Hotez, P. J. The intestinal protozoa: emerging impact on global health and development. *Curr. Opin. Gastroenterol.* **2015**, *31* (1), 38–44.
- (3) Pritt, B. S.; Clark, C. G. Amebiasis. *Mayo Clin. Proc.* **2008**, *83* (10), 1154–1160.
- (4) Ehrenkauf, G. M.; Suresh, S.; Solow-Cordero, D.; Singh, U. High-Throughput Screening of Entamoeba Identifies Compounds Which Target Both Life Cycle Stages and Which Are Effective Against Metronidazole Resistant Parasites. *Front. Cell Infect. Microbiol.* **2018**, *8*, 276.
- (5) Kikuchi, T.; Koga, M.; Shimizu, S.; Miura, T.; Maruyama, H.; Kimura, M. Efficacy and safety of paromomycin for treating amebiasis in Japan. *Parasitol. Int.* **2013**, *62* (6), 497–501.
- (6) Blessmann, J.; Tannich, E. Treatment of asymptomatic intestinal Entamoeba histolytica infection. *N. Engl. J. Med.* **2002**, *347* (17), 1384.
- (7) Cooper, C. J.; Fleming, R.; Boman, D. A.; Zuckerman, M. J. Varied Clinical Manifestations of Amebic Colitis. *South Med. J.* **2015**, *108* (11), 676–681.
- (8) Ceruelos, A. H.; Romero-Quezada, L. C.; Ruvalcaba Ledezma, J. C.; Lopez Contreras, L. Therapeutic uses of metronidazole and its side effects: an update. *Eur. Rev. Med. Pharmacol. Sci.* **2019**, *23* (1), 397–401.
- (9) Wassmann, C.; Hellberg, A.; Tannich, E.; Bruchhaus, I. Metronidazole resistance in the protozoan parasite Entamoeba histolytica is associated with increased expression of iron-containing superoxide dismutase and peroxiredoxin and decreased expression of ferredoxin 1 and flavin reductase. *J. Biol. Chem.* **1999**, *274* (37), 26051–26056.
- (10) Penuliar, G. M.; Nakada-Tsukui, K.; Nozaki, T. Phenotypic and transcriptional profiling in Entamoeba histolytica reveal costs to fitness and adaptive responses associated with metronidazole resistance. *Front. Microbiol.* **2015**, *6*, 354.
- (11) Bansal, D.; Sehgal, R.; Chawla, Y.; Malla, N.; Mahajan, R. C. Multidrug resistance in amoebiasis patients. *Indian J. Med. Res.* **2006**, *124* (2), 189–194.
- (12) Shirley, D. A. T.; Farr, L.; Watanabe, K.; Moonah, S. A Review of the Global Burden, New Diagnostics, and Current Therapeutics for Amebiasis. *Open Forum Infect. Dis.* **2018**, *5* (7), ofy161.
- (13) Shaulov, Y.; Sarid, L.; Trebicz-Geffen, M.; Ankri, S. Entamoeba histolytica Adaption to Auranofin: A Phenotypic and Multi-Omics Characterization. *Antioxidants* **2021**, *10* (8), 1240.
- (14) Rossignol, J. F.; Kabil, S. M.; El-Gohary, Y.; Younis, A. M. Nitazoxanide in the treatment of amoebiasis. *Trans. R. Soc. Trop. Med. Hyg.* **2007**, *101* (10), 1025–1031.
- (15) Nagaraja, S.; Ankri, S. Target identification and intervention strategies against amebiasis. *Drug Resistance Updates* **2019**, *44*, 1–14.
- (16) Martinez-Castillo, M.; Pacheco-Yepez, J.; Flores-Huerta, N.; Guzman-Tellez, P.; Jarillo-Luna, R. A.; Cardenas-Jaramillo, L. M.; Campos-Rodriguez, R.; Shibayama, M. Flavonoids as a Natural Treatment Against Entamoeba histolytica. *Front. Cell Infect. Microbiol.* **2018**, *8*, 209.
- (17) Menezes, S. A.; Tasca, T. Essential Oils and Terpenic Compounds as Potential Hits for Drugs against Amitochondriate Protists. *Trop. Med. Infect. Dis.* **2023**, *8* (1), 37.
- (18) Mori, M.; Tsuge, S.; Fukasawa, W.; Jeelani, G.; Nakada-Tsukui, K.; Nonaka, K.; Matsumoto, A.; Omura, S.; Nozaki, T.; Shiomi, K. Discovery of Antiamebic Compounds That Inhibit Cysteine Synthase From the Enteric Parasitic Protist Entamoeba histolytica by Screening of Microbial Secondary Metabolites. *Front. Cell Infect. Microbiol.* **2018**, *8*, 409.
- (19) Mehlotra, R. K. Antioxidant defense mechanisms in parasitic protozoa. *Crit. Rev. Microbiol.* **1996**, *22* (4), 295–314.
- (20) Tekwani, B. L.; Mehlotra, R. K. Molecular basis of defence against oxidative stress in and. *Microbes Infect.* **1999**, *1* (5), 385–394.
- (21) Dingsdag, S. A.; Hunter, N. Metronidazole: an update on metabolism, structure-cytotoxicity and resistance mechanisms. *J. Antimicrob. Chemother.* **2018**, *73* (2), 265–279.
- (22) Muller, M. Reductive activation of nitroimidazoles in anaerobic microorganisms. *Biochem. Pharmacol.* **1986**, *35* (1), 37–41.
- (23) Edwards, D. I. Reduction of nitroimidazoles in vitro and DNA damage. *Biochem. Pharmacol.* **1986**, *35* (1), 53–58.
- (24) Edwards, D. I. Nitroimidazole drugs-action and resistance mechanisms I. Mechanism of action. *J. Antimicrob. Chemother.* **1993**, *31* (1), 9–20.
- (25) Leitsch, D.; Kolarich, D.; Binder, M.; Stadlmann, J.; Altmann, F.; Duchene, M. Trichomonas vaginalis: metronidazole and other nitroimidazole drugs are reduced by the flavin enzyme thioredoxin reductase and disrupt the cellular redox system. Implications for nitroimidazole toxicity and resistance. *Mol. Microbiol.* **2009**, *72* (2), 518–536.
- (26) Wassmann, C.; Bruchhaus, I. Superoxide dismutase reduces susceptibility to metronidazole of the pathogenic protozoan Entamoeba histolytica under microaerophilic but not under anaerobic conditions. *Arch. Biochem. Biophys.* **2000**, *376* (1), 236–238.
- (27) Samarawickrema, N. A.; Brown, D. M.; Upcroft, J. A.; Thammapalerd, N.; Upcroft, P. Involvement of superoxide dismutase and pyruvate:ferredoxin oxidoreductase in mechanisms of metronidazole resistance in Entamoeba histolytica. *J. Antimicrob. Chemother.* **1997**, *40* (6), 833–840.
- (28) Leitsch, D. Drug susceptibility testing in microaerophilic parasites: Cysteine strongly affects the effectiveness of metronidazole and auranofin, a novel and promising antimicrobial. *Int. J. Parasitol.: Drugs Drug Resist.* **2017**, *7* (3), 321–327.
- (29) Leitsch, D.; Williams, C. F.; Hrdy, I. Redox Pathways as Drug Targets in Microaerophilic Parasites. *Trends Parasitol.* **2018**, *34* (7), 576–589.
- (30) Cabeza, M. S.; Guerrero, S. A.; Iglesias, A. A.; Arias, D. G. New enzymatic pathways for the reduction of reactive oxygen species in Entamoeba histolytica. *Biochim. Biophys. Acta* **2015**, *1850* (6), 1233–1244.
- (31) Chen, J.; Huang, X.; Liu, Y.; Dai, G.; Chen, W. Detoxifying enzymes of Entamoeba histolytica and their detoxifying roles. *Chin. Med. J.* **1996**, *109* (10), 792–794.
- (32) Jeelani, G.; Nozaki, T. Entamoeba thiol-based redox metabolism: A potential target for drug development. *Mol. Biochem. Parasitol.* **2016**, *206* (1–2), 39–45.
- (33) Ali, V.; Nozaki, T. Current therapeutics, their problems, and sulfur-containing-amino-acid metabolism as a novel target against infections by "amitochondriate" protozoan parasites. *Clin. Microbiol. Rev.* **2007**, *20* (1), 164–187.
- (34) Fahey, R. C.; Newton, G. L.; Arrick, B.; Overdank-Bogart, T.; Aley, S. B. Entamoeba histolytica: a eukaryote without glutathione metabolism. *Science* **1984**, *224* (4644), 70–72.
- (35) Vanacova, S.; Liston, D. R.; Tachezy, J.; Johnson, P. J. Molecular biology of the amitochondriate parasites, Giardia intestinalis, Entamoeba histolytica and Trichomonas vaginalis. *Int. J. Parasitol.* **2003**, *33* (3), 235–255.
- (36) Lithgow, J. K.; Hayhurst, E. J.; Cohen, G.; Aharonowitz, Y.; Foster, S. J. Role of a cysteine synthase in Staphylococcus aureus. *J. Bacteriol.* **2004**, *186* (6), 1579–1590.
- (37) Sareen, D.; Newton, G. L.; Fahey, R. C.; Buchmeier, N. A. Mycothiol is essential for growth of Mycobacterium tuberculosis Erdman. *J. Bacteriol.* **2003**, *185* (22), 6736–6740.
- (38) Bornemann, C.; Jardine, M. A.; Spies, H. S.; Steenkamp, D. J. Biosynthesis of mycothiol: elucidation of the sequence of steps in Mycobacterium smegmatis. *Biochem. J.* **1997**, *325* (3), 623–629.
- (39) Hung, J.; Cooper, D.; Turner, M. S.; Walsh, T.; Giffard, P. M. Cystine uptake prevents production of hydrogen peroxide by Lactobacillus fermentum BR11. *FEMS Microbiol. Lett.* **2003**, *227* (1), 93–99.
- (40) Even, S.; Burguière, P.; Auger, S.; Soutourina, O.; Danchin, A.; Martin-Verstraete, I. Global control of cysteine metabolism by CymR in Bacillus subtilis. *J. Bacteriol.* **2006**, *188* (6), 2184–2197.
- (41) Hochgrafe, F.; Mostertz, J.; Pother, D. C.; Becher, D.; Helmann, J. D.; Hecker, M. S-cysteinylation is a general mechanism for thiol protection of Bacillus subtilis proteins after oxidative stress. *J. Biol. Chem.* **2007**, *282* (36), 25981–25985.

- (42) Kumar, S.; Tripathi, L. M.; Sagar, P. Oxido-reductive functions of Entamoeba histolytica in relation to virulence. *Ann. Trop. Med. Parasitol.* **1992**, *86* (3), 239–248.
- (43) Brunner, K.; Maric, S.; Reshma, R. S.; Almqvist, H.; Seashore-Ludlow, B.; Gustavsson, A. L.; Poyraz, O.; Yogeewari, P.; Lundback, T.; Vallin, M.; Sriram, D.; Schnell, R.; Schneider, G. Inhibitors of the Cysteine Synthase CysM with Antibacterial Potency against Dormant Mycobacterium tuberculosis. *J. Med. Chem.* **2016**, *59* (14), 6848–6859.
- (44) Spyraakis, F.; Singh, R.; Cozzini, P.; Campanini, B.; Salsi, E.; Felici, P.; Raboni, S.; Benedetti, P.; Cruciani, G.; Kellogg, G. E.; Cook, P. F.; Mozzarelli, A. Isozyme-specific ligands for O-acetylserine sulfhydrylase, a novel antibiotic target. *PLoS One* **2013**, *8* (10), No. e77558.
- (45) Dharavath, S.; Raj, I.; Gourinath, S. Structure-based mutational studies of O-acetylserine sulfhydrylase reveal the reason for the loss of cysteine synthase complex formation in Brucella abortus. *Biochem. J.* **2017**, *474* (7), 1221–1239.
- (46) Salsi, E.; Bayden, A. S.; Spyraakis, F.; Amadasi, A.; Campanini, B.; Bettati, S.; Dodatko, T.; Cozzini, P.; Kellogg, G. E.; Cook, P. F.; Roderick, S. L.; Mozzarelli, A. Design of O-acetylserine sulfhydrylase inhibitors by mimicking nature. *J. Med. Chem.* **2010**, *53*, 345–356.
- (47) Kant, V.; Vijayakumar, S. A.-O.; Sahoo, G. C.; Ali, V.; Singh, K.; Chaudhery, S. S.; Das, P. In-silico screening and validation of high-affinity tetra-peptide inhibitor of Leishmania donovani O-acetyl serine sulfhydrylase (OASS). *J. Biomol. Struct. Dyn.* **2019**, *37*, 481–492.
- (48) Mazumder, M.; Gourinath, S. Structure-Based Design of Inhibitors of the Crucial Cysteine Biosynthetic Pathway Enzyme O-Acetyl Serine Sulfhydrylase. *Top. Med. Chem.* **2015**, *16*, 948–959.
- (49) Nagpal, I.; Raj, I.; Subbarao, N.; Gourinath, S. Virtual screening, identification and in vitro testing of novel inhibitors of O-acetyl-L-serine sulfhydrylase of Entamoeba histolytica. *PLoS One* **2012**, *7* (2), No. e30305.
- (50) Agarwal, S. M.; Jain, R.; Bhattacharya, A.; Azam, A. Inhibitors of Escherichia coli serine acetyltransferase block proliferation of Entamoeba histolytica trophozoites. *Int. J. Parasitol.* **2008**, *38* (2), 137–141.
- (51) Kumari, P.; Babuta, M.; Bhattacharya, A.; Gourinath, S. Structural and functional characterisation of phosphoserine phosphatase, that plays critical role in the oxidative stress response in the parasite Entamoeba histolytica. *J. Struct. Biol.* **2019**, *206* (2), 254–266.
- (52) Jang, J.; Chang, J. H. Molecular Structure of Phosphoserine Aminotransferase from Saccharomyces cerevisiae. *Int. J. Mol. Sci.* **2023**, *24* (6), 5139.
- (53) Marchesani, F.; Zangelmi, E.; Murtas, G.; Costanzi, E.; Ullah, R.; Peracchi, A.; Bruno, S.; Pollegioni, L.; Mozzarelli, A.; Storici, P.; Campanini, B. L-serine biosynthesis in the human central nervous system: Structure and function of phosphoserine aminotransferase. *Protein Sci.* **2023**, *32* (4), No. e4609.
- (54) Singh, R. K.; Kumar, D.; Gourinath, S. Phosphoserine Aminotransferase has Conserved Active Site from Microbes to Higher Eukaryotes with Minor Deviations. *Protein Pept. Lett.* **2021**, *28* (9), 996–1008.
- (55) Singh, R. K.; Raj, I.; Pujari, R.; Gourinath, S. Crystal structures and kinetics of Type III 3-phosphoglycerate dehydrogenase reveal catalysis by lysine. *FEBS J.* **2014**, *281* (24), 5498–5512.
- (56) Ali, V.; Hashimoto, T.; Shigeta, Y.; Nozaki, T. Molecular and biochemical characterization of D-phosphoglycerate dehydrogenase from Entamoeba histolytica. A unique enteric protozoan parasite that possesses both phosphorylated and nonphosphorylated serine metabolic pathways. *Eur. J. Biochem.* **2004**, *271* (13), 2670–2681.
- (57) Mishra, V.; Kumar, A.; Ali, V.; Nozaki, T.; Zhang, K. Y.; Bhakuni, V. Glu-108 is essential for subunit assembly and dimer stability of D-phosphoglycerate dehydrogenase from Entamoeba histolytica. *Mol. Biochem. Parasitol.* **2012**, *181* (2), 117–124.
- (58) Mishra, V.; Kumar, A.; Ali, V.; Nozaki, T.; Zhang, K. Y.; Bhakuni, V. Novel protein-protein interactions between Entamoeba histolyticad-phosphoglycerate dehydrogenase and phosphoserine aminotransferase. *Biochimie* **2012**, *94* (8), 1676–1686.
- (59) Singh, R. K.; Tomar, P.; Dharavath, S.; Kumar, S.; Gourinath, S. N-terminal residues are crucial for quaternary structure and active site conformation for the phosphoserine aminotransferase from enteric human parasite E. histolytica. *Int. J. Biol. Macromol.* **2019**, *132*, 1012–1023.
- (60) Ali, V.; Nozaki, T. Biochemical and functional characterization of phosphoserine aminotransferase from Entamoeba histolytica, which possesses both phosphorylated and non-phosphorylated serine metabolic pathways. *Mol. Biochem. Parasitol.* **2006**, *145* (1), 71–83.
- (61) Mishra, V.; Ali, V.; Nozaki, T.; Bhakuni, V. Entamoeba histolytica Phosphoserine aminotransferase (EhPSAT): insights into the structure-function relationship. *BMC Res. Notes* **2010**, *3*, 52.
- (62) Chiba, Y.; Makiuchi, T.; Jeelani, G.; Nozaki, T. Heterogeneity of the serine synthetic pathway in Entamoeba species. *Mol. Biochem. Parasitol.* **2016**, *207* (2), 56–60.
- (63) Kumari, P.; Vijayan, R.; Gourinath, S. Structural analysis of EhPSP in complex with 3-phosphoglyceric acid from Entamoeba histolytica reveals a basis for its lack of phosphoglycerate mutase activity. *Int. J. Biol. Macromol.* **2021**, *178*, 1–10.
- (64) Madhavi Sastry, G.; Adzhigirey, M.; Day, T.; Annabhimoju, R.; Sherman, W. Protein and ligand preparation: parameters, protocols, and influence on virtual screening enrichments. *J. Comput.-Aided Mol. Des.* **2013**, *27* (3), 221–234.
- (65) Friesner, R. A.; Murphy, R. B.; Repasky, M. P.; Frye, L. L.; Greenwood, J. R.; Halgren, T. A.; Sanschagrin, P. C.; Mainz, D. T. Extra precision glide: docking and scoring incorporating a model of hydrophobic enclosure for protein-ligand complexes. *J. Med. Chem.* **2006**, *49* (21), 6177–6196.
- (66) Lyne, P. D.; Lamb, M. L.; Saeh, J. C. Accurate prediction of the relative potencies of members of a series of kinase inhibitors using molecular docking and MM-GBSA scoring. *J. Med. Chem.* **2006**, *49* (16), 4805–4808.
- (67) Baykov, A. A.; Evtushenko, O. A.; Avaeva, S. M. A malachite green procedure for orthophosphate determination and its use in alkaline phosphatase-based enzyme immunoassay. *Anal. Biochem.* **1988**, *171* (2), 266–270.
- (68) Motulsky, H. J. *Prism 5 Statistics Guide*; GraphPad Prism: San Diego CA, 2007.
- (69) Bowers, K. J.; C, E.; Xu, H.; Dror, R. O.; Eastwood, M. P.; Gregersen, B. A.; Klepeis, J. L.; Kolossvary, I.; Moraes, M. A.; Sacerdoti, F. D.; et al. Scalable algorithms for molecular dynamics simulations on commodity clusters In *Proceedings of the 2006 ACM/IEEE conference on Supercomputing*; SC '06; Association for Computing Machinery: New York, NY, USA, 2006.
- (70) Laskowski, R. A.; Swindells, M. B. LigPlot+: multiple ligand-protein interaction diagrams for drug discovery. *J. Chem. Inf. Model.* **2011**, *51* (10), 2778–2786.
- (71) Wallace, A. C.; Laskowski, R. A.; Thornton, J. M. LIGPLOT: a program to generate schematic diagrams of protein-ligand interactions. *Protein Eng.* **1995**, *8* (2), 127–134.
- (72) Daina, A.; Michielin, O.; Zoete, V. SwissADME: a free web tool to evaluate pharmacokinetics, drug-likeness and medicinal chemistry friendliness of small molecules. *Sci. Rep.* **2017**, *7*, 42717.
- (73) Husain, A.; Sato, D.; Jeelani, G.; Mi-ichi, F.; Ali, V.; Suematsu, M.; Soga, T.; Nozaki, T. Metabolome analysis revealed increase in S-methylcysteine and phosphatidylisopropanolamine synthesis upon L-cysteine deprivation in the anaerobic protozoan parasite Entamoeba histolytica. *J. Biol. Chem.* **2010**, *285* (50), 39160–39170.
- (74) Gillin, F. D.; Diamond, L. S. Entamoeba histolytica and Giardia lamblia: effects of cysteine and oxygen tension on trophozoite attachment to glass and survival in culture media. *Exp. Parasitol.* **1981**, *52* (1), 9–17.
- (75) Jeelani, G.; Husain, A.; Sato, D.; Ali, V.; Suematsu, M.; Soga, T.; Nozaki, T. Two atypical L-cysteine-regulated NADPH-dependent oxidoreductases involved in redox maintenance, L-cystine and iron reduction, and metronidazole activation in the enteric protozoan Entamoeba histolytica. *J. Biol. Chem.* **2010**, *285* (35), 26889–26899.
- (76) Husain, A.; Jeelani, G.; Sato, D.; Nozaki, T. Global analysis of gene expression in response to L-Cysteine deprivation in the anaerobic protozoan parasite Entamoeba histolytica. *BMC Genomics* **2011**, *12*, 275.

(77) Jeelani, G.; Sato, D.; Soga, T.; Watanabe, H.; Nozaki, T. Mass spectrometric analysis of L-cysteine metabolism: physiological role and fate of L-cysteine in the enteric protozoan parasite *Entamoeba histolytica*. *mBio* **2014**, *5* (6), No. e01995.

(78) Mori, M.; Jeelani, G.; Masuda, Y.; Sakai, K.; Tsukui, K.; Waluyo, D.; Tarwadi; Watanabe, Y.; Nonaka, K.; Matsumoto, A.; Omura, S.; Nozaki, T.; Shiomi, K. Identification of natural inhibitors of *Entamoeba histolytica* cysteine synthase from microbial secondary metabolites. *Front. Microbiol.* **2015**, *6*, 962.

(79) Jeelani, G.; Sato, D.; Soga, T.; Nozaki, T. Genetic, metabolomic and transcriptomic analyses of the de novo L-cysteine biosynthetic pathway in the enteric protozoan parasite *Entamoeba histolytica*. *Sci. Rep.* **2017**, *7* (1), 15649.

(80) Arora, G.; Tiwari, P.; Mandal, R. S.; Gupta, A.; Sharma, D.; Saha, S.; Singh, R. High throughput screen identifies small molecule inhibitors specific for *Mycobacterium tuberculosis* phosphoserine phosphatase. *J. Biol. Chem.* **2014**, *289* (36), 25149–25165.